Chapter 19

Plasmonic Rectenna for Efficient Conversion of Light into Electricity

Fuyi Chen, Jian Liu and Negash Alemu

Additional information is available at the end of the chapter

http://dx.doi.org/10.5772/51045

1. Introduction

Solar energy has been widely studied as a green energy source. Present photovoltaic techniques are mainly semiconductor solar cells. The silicon solar cell has a good power conversion efficiency of 24%, and the semiconductor solar cell based on GaAs multijunction has the highest conversion efficiency of 32% at present [1]. Though these semiconductor solar cells have relatively high conversion efficiency, their high cost and some poisonous byproduct produced during the manufacturing process limit their commercial use. As an alternative for large scale application, the dye-sensitized solar cell (DSSC) has obtained conversion efficiency of 12% at maximum in these days [2], only a few percentages has been increased since the Grazel's research, in which the conversion efficiency of DSSC is improved using nanoporous photoanodes [3].

In 1998, Stuart et al. [4] reported the first application of surface plasmons in the photovoltaic technology. It was found that the photocurrent of the thin-film Silicon-on-insulator (SOI) device was 18 times improved at the wavelength of 800 nm by metallic nanoparticles. So far, the plasmonic effect of the metal nanostructure is one of the main directions [5, 6] to improve the conversion efficiency for DSSC. The United States of America (USA), the European Union and many other countries undertake some related projects, such as the SOLAMON project, and some typical research achievements are obtained in the plasmonic DSSC field, which are described as follows according to the role of metal surface plasmons:

Scattering effect of localized surface plasmon resonance (LSPR). Brown et al. [7] reported that adding Au-Si nanoparticles with the shell-core structure with size of 20 nm into the typical solid electrolyte DSSC led to an improvement of the conversion efficiency; Hagglund et al. [8] studied the influence of Au nanoplate arrays on the photoelectric conduction of the dye-sensitized TiO_2 thin-film.

Concentration effect of light using localized surface plasmon resonance (LSPR). Du et al. [9] theoretically demonstrated that the Au nanodimer improved the ultraviolet absorption of the TiO_2 nanoparticles; Guilatt et al. [10] studied the light absorption property of the Au nanoshell in the Si thin-film.

Trapping effect of surface plasmon polariton (SPP). Fu et al. [11] reported the conversion efficiency of the typical DSSC with the Pt fishnet arrays as the counter electrode, Durr et al. [12] studied the effect of the Ag thin-film on the short circuit current in DSSC with a planar waveguide structure.

It is clear that metallic nanostructures possess the excellent light-harvesting capability in the visible spectrum, and they can collect almost all the photon energy which is concentrated on the nanoscale plasmonic hotspots from an incident light wavelength region of several hundred nanometers. Therefore, the electromagnetic fields in these regions are enhanced exponentially.

However, the total energy conversion efficiency of DSSC with the plasmonic optical effect is not increased simultaneously as we expect. As shown in the experiments, the power conversion efficiencies were only 1.95 % [7] and 5.77 % [11] with the plasmonic effect considered. We show in next section that the parasitic absorption of small metal nanoparticles is the main reason, and the power conversion efficiency enhanced by metallic nanoparticles is much less than their enhanced efficiency of light collection because the metallic nanoparticles absorb one part of the incident light during surface plasmon resonance (SPR). The parasitic absorption had been mentioned in previous thin film devices [13, 14] which demonstrated that the metallic absorption had an adverse effect on the solar cell performance.

2. Parasitic absorption of metal nanoparticles in the plasmonic DSSC

Our numerical calculations were performed using the finite difference time domain technique (FDTD) to solve the three-dimensional vector Maxwell equations in the optical structure of the plasmonic DSSC, as showed in Figure 1. The distance of the two transparent conductive oxides (TCO) electrodes was 1600 nm, the dye-sensitized layer was 500 nm in thickness. The FCC-arranged Ag spherical nanoparticle array was on top of the dye-sensitized layer with a 2 nm space. The plasmonic DSSC was illuminated with plane wave from the top TCO cathode with the electric field in the Ag spherical nanoparticle array. A perfectly matched layer and a conformal mesh region self-adapted to the structure were used.

The transmission parameters were calculated as the ratio of the power transmitted through the structure to the power incident, and the reflection parameters were calculated as the ratio of the power reflected from the structure to the power incident. The particle swarm optimization (PSO) was used to evaluate different design geometries to locate an optimum solution. PSO, based on the movement and intelligence of swarms, was a robust stochastic evolutionary computation technique inspired in the behavior of bee flocks [15]. It has been shown in certain instances to outperform other methods of optimization like genetic algorithms (GA) in the electromagnetic community [16].

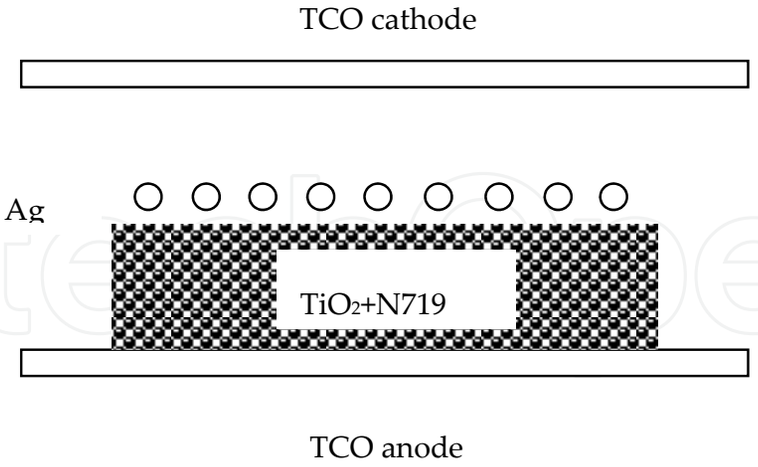

Figure 1. Schematic of the plasmonic DSSC structure. Dye-sensitized layer is 500 nm in thickness, Ag nanoparticle is 210 nm in diameter, the spacing between sensitized layer and Ag nanoparticles is 2 nm, the distance of the two transparent conductive oxides (TCO) electrodes is 1600 nm.

Figure 2 shows the monochromatic absorption enhancement and the integral quantum efficiency (IQE) enhancement as a function of Ag nanoparticles diameter and period of the Ag nanoparticles arrays in the wavelength range of 400~1100 nm. The optimal optical structure designed based on PSO for the present study is the Ag nanoparticles array of 210 nm in diameter and 500 nm in period, which has an improved integral quantum efficiency (IQE) enhancement of 11.3%. The monochromatic absorption enhancement of the Ag nanoparticles of diameter = 210 nm and period = 500 nm is improved by 20-30 % in the wavelength range 630 nm to 1100 nm, it has a maximum enhancement of absorption at the wavelength of 796 nm, and it is far higher than that of the Ag nanoparticle arrays of diameter = 70 nm and period = 250 nm which does not improve the conversion efficiency significantly.

Figure 3 shows the optical properties, the electric near-field distribution and the visible light absorption distribution at wavelength of 796 nm in the optimized plasmonic DSSC. It can be seen from Figure 3 (left) that even under optimization condition the metal absorption takes up 20-30 % of total absorption in the visible bands of 400-700 nm, which is consistent with the monochromatic absorption enhancement spectrum. This may be because of the electric field is mainly distributed at the outside of the Ag nanoparticles, and the metal nanoparticle absorption intensity is higher than the dyes, which can be seen from Figure 3 (right). It is clear from Figure 3 (middle) that the silver particle increases absorption of the dye by the enhanced forward scattering due to the surface plasmon resonance.

Although the conversion efficiency of photoactiviated thin film can be improved by about 15-20% theoretically by optimized metal nanoparticle arrays, the absorption of metal nanoparticles (210 nm in diameter) take up about 20-30% of total absorption of the DSSC in visible light, *i.e.*, lights absorbed by DSSC does not completely convert into photocurrent. A part of the energy is lost in the form of Joule heat (ohmic loss), which led to the low external quantum efficiency of photoelectric conversion.

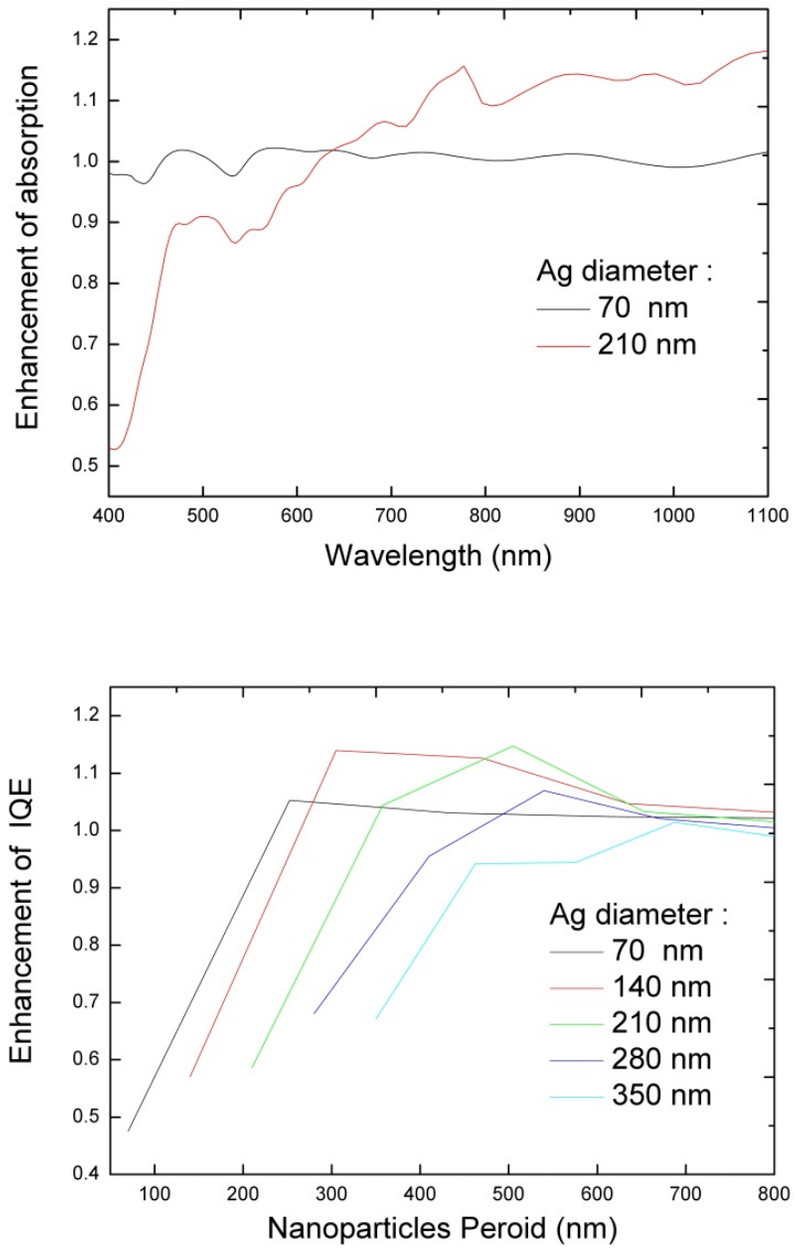

Figure 2. (a) Monochromatic light absorption enhancement of the Ag nanoparticle arrays of 70 nm and 210 nm in diameter and (b) the integral quantum efficiency enhancement of Ag nanoparticle arrays with different period (70-800 nm) and diameter (70-210 nm).

In typical DSSC device, the dye sensitized TiO_2 is 10-80 nm in diameter [17], in order to build the electrostatic localized surface plasmon resonances of metallic nanoparticles inside the dye sensitized TiO_2, the smaller Ag nanoparticles were buried to improve the absorption of dye sensitized TiO_2 nanoparticles, the intrinsic heat loss of small metal nanoparticles (such as 70 nm) at visible light bands is far greater than the electromagnetic energy scattered into the optical activity medium by these metal nanoparticles. The problem has to be considered in the plasmonic DSSC device, which has been highlighted in a recent review [18].

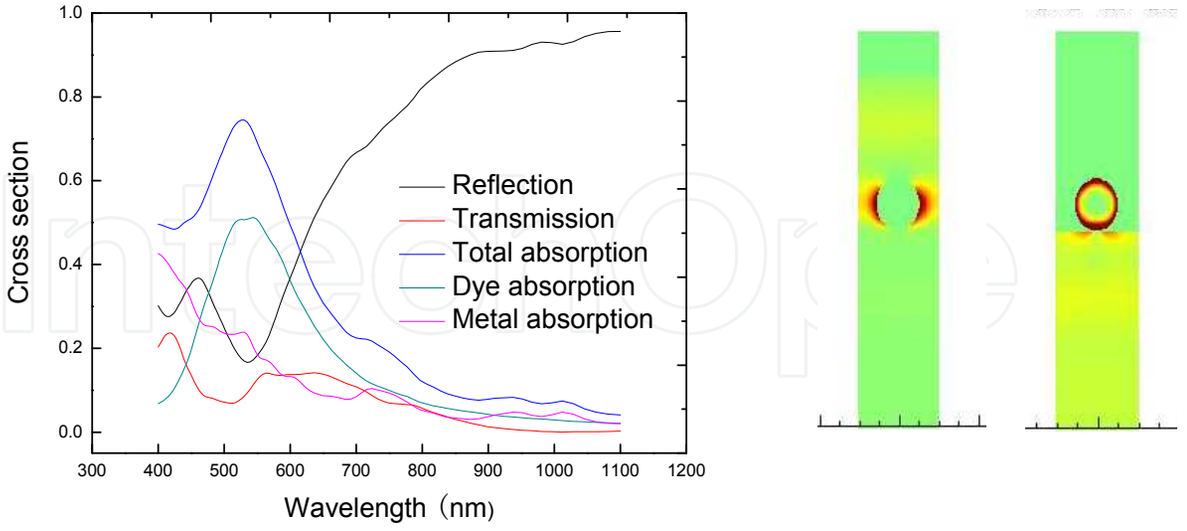

Figure 3. Optical properties of the plasmonic DSSC (left) under optimized conditions (Ag diameter of 210 nm, period 500 nm), the electric near-field distribution (middle) and the visible light absorption distribution (right) in DSSC at wavelength of 796 nm where the enhancement of monochromatic absorption is maximum.

To solve the problem of metal parasitic absorption in DSSC caused by surface plasmon optical effect, Guilatt et al. [10] theoretically studied the method of using metal shell-core nanostructure to substitute pure metal nanoparticles. But the potential development of this method was limited by the metallic skin absorption property. Designing and fabricating the metal-insulator-metal (MIM) sandwich structure optical rectenna as photon acceptor and electron donor may be a research direction for the further development of the plasmonic photovoltaic techniques. In this chapter, we further develop the idea of optical rectification (OR) that can convert visible/near-infrared (VIS/NIR) wavelengths to direct current. Section 3 includes the antenna properties of the noble metal (Ag) and transition metal (Ti), and metal-insulator-metal (MIM) nanostructure and Section 4 includes the optical rectification properties of Ag-TiO_2-Ti and AgCu-TiO_2/Ti metal-insulator-metal (MIM) diode devices. We exploit these contents to address the effect of plasmonic properties on the electronic transport behaviors in noble-transition metal heterodimers in order to put forth a new theory on the plasmonic optical rectification.

3. Antenna properties of the noble, transition metal nanowires, metal-insulator-metal (MIM) nanostructures

3.1. Review of optical rectification (OR) effect

Metallic nanostructures provide a means to transduce free-propagating electromagnetic waves into localized surface plasmon resonance modes [19] and can function as optical antennas [20]. In the traditional radiofrequency and microwave regime, antennas (such as antennas in mobile phones of our everyday life) are usually used to convert electromagnetic

radiations into electric currents, however, most of the optical antennas studied so far operate on a "light-in and light-out" basis [21], the utilizing of metallic optical antennas to convert the optical radiations into photocurrents is one of the most imperative tasks for the state-of-the-art plasmonic technology. Conversion of visible/near-infrared (VIS/NIR) wavelengths to effective direct currents (DC) is a second-order nonlinear optical phenomena, e.g., optical rectification (OR) effect.

The search for OR effect in metallic optical antennas was started in 1964, when Brown of the Raytheon Company demonstrated the first flight of a microwave-powered helicopter using rectenna [22], a high up to 90% efficiency was obtained for a rectenna operating at single microwave frequency in 1976 [23]. Generally speaking, the OR effect could achieve up to 80 percent efficiency of energy conversion and power transmission in microwave range 300 MHz to 300 GHz, and typical antenna structure size was around few millimeters.

The endeavor for conversion of light radiation to DC power was started in 1968 [24], following the example of the microwave point-contact diode rectification structure, much research has been performed to extend the concept and application of rectenna into ultrahigh (visible) frequencies (1000THz), and progress has been made in the fabrication and characterization of the metal-insulator-metal (MIM) diodes for use in rectification device. It has been demonstrated that optical antennas can couple electromagnetic radiation in the visible in the same way as radio antennas do at their corresponding wavelength, three kinds of the metallic nanostructures with OR effect in the visible/near-infrared wavelength range had been located: whisker diodes [24,25], Schottky diodes [26,27] and metal-insulator-metal tunneling diodes [28,29]. Meanwhile, for the application in the solar cell technology, Bailey originally proposed that broadband rectifying antennas can be used for direct conversion of solar energy to DC power [30], the first patent on solar rectification was issued to Marks [31].

It is clear that metallic optical antennas possess as good capability of receiving electromagnetic energy in the visible/near-infrared spectrum as the radiofrequency antennas do, and that they can collect almost all the photon energy in a wavelength range of several hundreds of nanometers. However, in comparison with the high conversion efficiency of the radio frequency antennas, the theory and application of OR effect of visible and infrared radiation is still in its infancy, a major technological difficulties that impede the performance of OR device at high frequency is that in the infrared and visible wavelength, metals are no longer perfect conductor.

The main difference between low frequency and ultrahigh frequencies electromagnetic waves when it comes to interaction with the free electrons in a finite piece of metal is the fact that electrons have an effective mass which causes them to react with increasing phase lag to an oscillating electromagnetic field as the frequency increases. For increasing frequency of the excitation, they exhibit an increasing oscillation amplitude as well as an increasing phase lag. As soon as the phase lag approaches 90^{o} the amplitude of the charge oscillation goes through a maximum and is only limited by the internal (ohmic and radiation) damping of the system.

This resonance corresponds to the surface plasmon resonance, for certain metals (such as gold, silver and copper) which consist of the anode and cathode in the metal-insulator-metal (MIM) structure optical rectennas, the surface plasmon resonance happens to appear in or

close to the visible spectral range. Plasmon resonances do not appear in perfect conductors (metals at low enough frequencies) since in those materials by definition no phase lag exists between excitation and charge response. The presence of plasmon resonance is therefore characteristic for optical frequencies and give rise to drawbacks of antenna systems in this frequency range, such as enhance Ohmic losses compared to the radiofrequency regime.

3.2. Modeling of the nanowire antenna

Nanowires which are made up of either noble or transition metals exhibit distinctive electromagnetic properties that make them appropriate candidate for nanoantenna at higher frequencies. This nanoantenna is put to practical application for efficient conversion of visible-near infrared spectrum energy into direct current electricity since its operation is on the basis of the wave nature of optical radiation.

In this section, long vertical nanowires were theoretically investigated as a model system to understand the behavior of dipole optical antennas. Figure 4(a) shows the geometry of the nanowire structure. The nanowire consists of the perfectly conductor (PEC), silver (Ag) or titanium (Ti) with the diameter of 100 nm and the length of 2000 nm. The plane wave source is located to the left of the structures in vacuum. The results of field enhancement and vertical components of the Poynting vector of antenna radiation simulations are depicted in Figures 5-11.

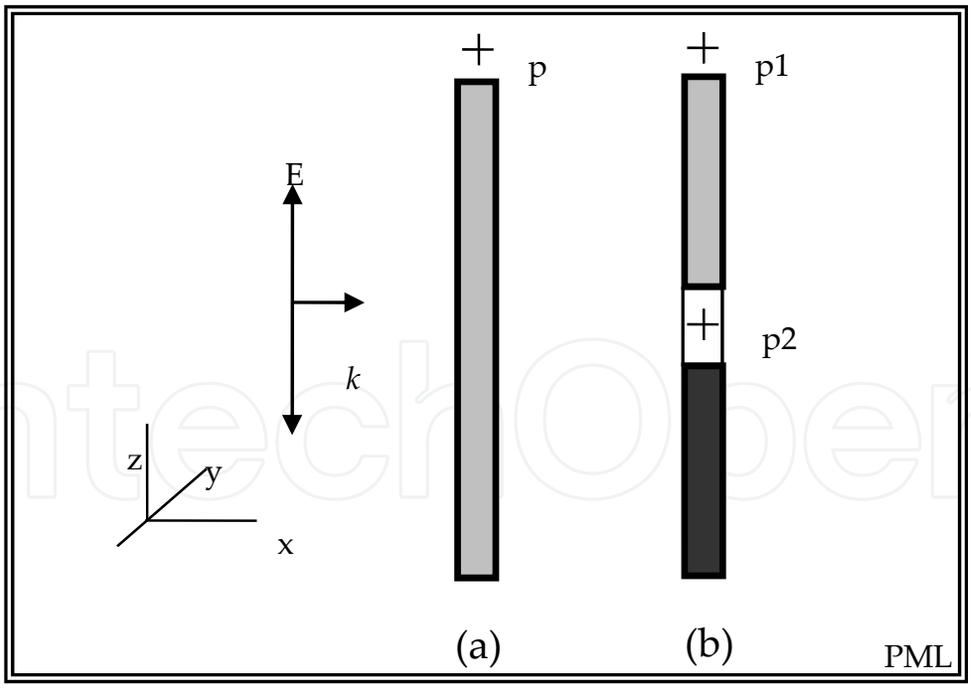

Figure 4. Schematic of the nanowire (a) and its heterodimer (b) as the calculation model for the antenna properties using the finite difference time domain (FDTD) method. The polarization direction (E) is along the long symmetric axis of the nanowires. The position of p and p1 are 5 nm from the nanowire apex, and p2 is at the middle of the dimer. The mesh is truncated using PML absorbing boundary conditions.

3.3. Perfectly conducting nanowire

According to classical antenna theory, metal antennas resonate at a wavelength λ when their length equals approximately $(2n+1)\lambda/2$, where n=0, 1, 2, etc. At resonance the charge distribution inside the antenna intensifies the incident electric field (E-field) locally at its end. In Figure 5 and 6, we plot the calculated values for the field enhancement $|E|/|E_0|$, normalized to the incident electric field, at the apex of the nanorod, for a 2000 nm perfectly conducting nanowires.

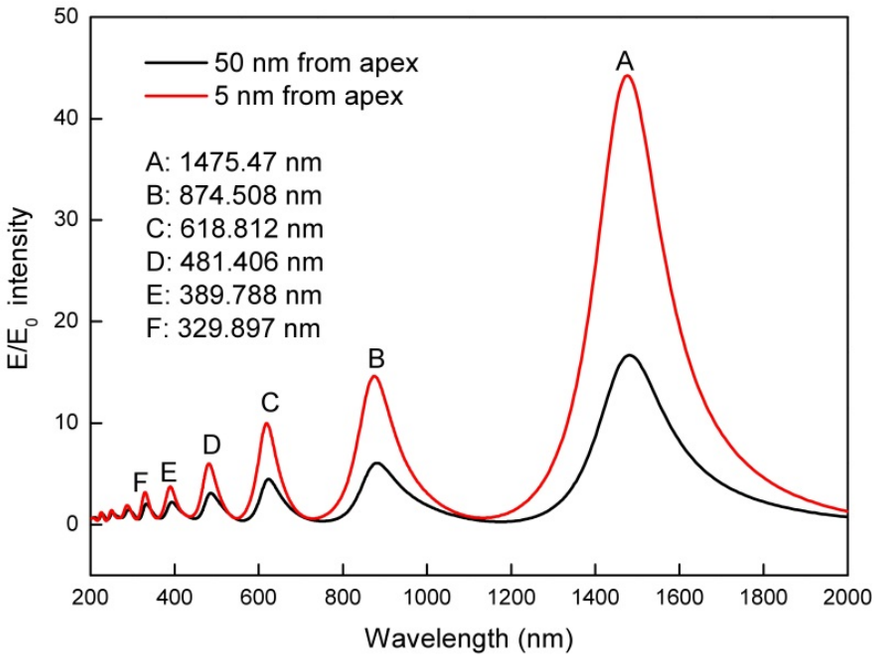

Figure 5. Multiple resonance spectrum around a perfectly conducting nanowire. The resonance is shown as a value of $|E|/|E_0|$ at a point of 5 or 50 nm above the nanowire as a function of wavelength of incident light (200 nm to 2000 nm).

Figure 5 and 6 show the simulated local field intensity enhancement spectra for perfectly conducting nanowire, its intensity distribution and Poynting vector corresponding to the higher harmonic mode resonances. Multiple resonances have seen in the field enhancement spectrum (Figure 5) at the given wavelength range. Each resonance corresponds to specific harmonic modes in the near field.

3.4. Ag nanowire

Any specific structure to consider as an optical antenna is supposed to be able to localize and enhance the propagating electromagnetic wave within a certain bandwidth. The results for silver nanowire with the parameters mentioned above are presented in Figure 7, 8 and 11. The results show that silver nanowire has enhancement spectra with very distinct peaks. The peak at shorter wavelength (350.477nm) attributed to surface plasmon resonance and for the wavelengths in the remaining band strong multiple resonances are observed.

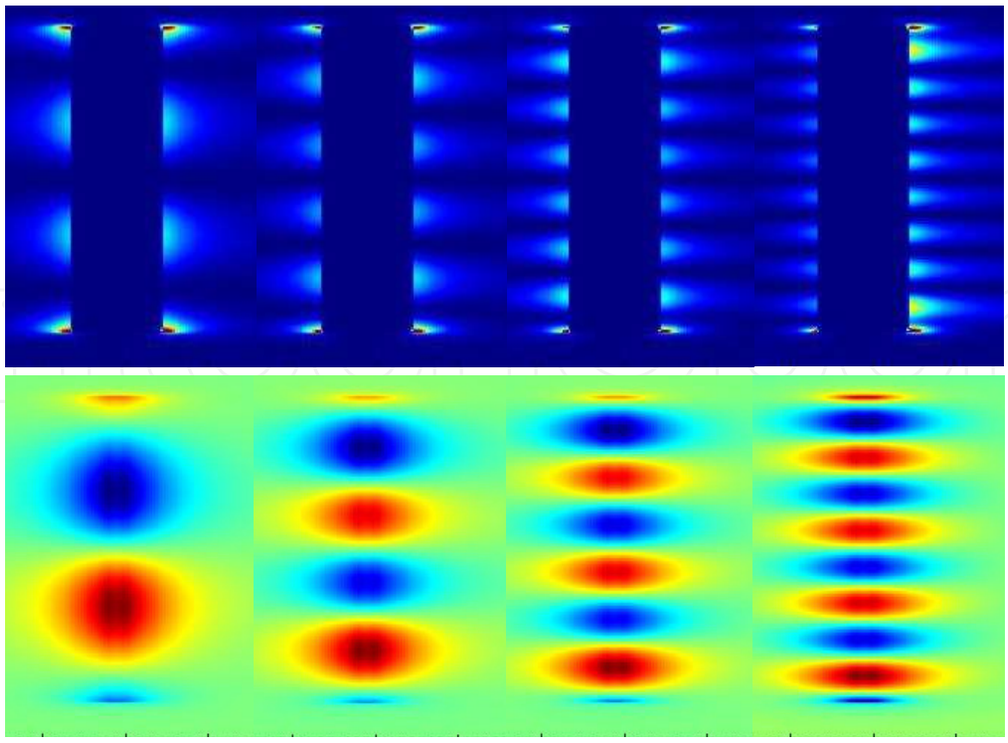

Figure 6. Simulated results for electric field profiles (top four panels) and vertical components of the Poynting vector of antenna radiations (bottom four panels) around a perfectly conducting nanowire, corresponding to the antenna mode (3λ/2, 5λ/2, 7λ/2 and 9λ/2 resonances). The electric field profile running through the center of the nanowires and the Poynting vector calculated at 55 nm above the nanowire axis.

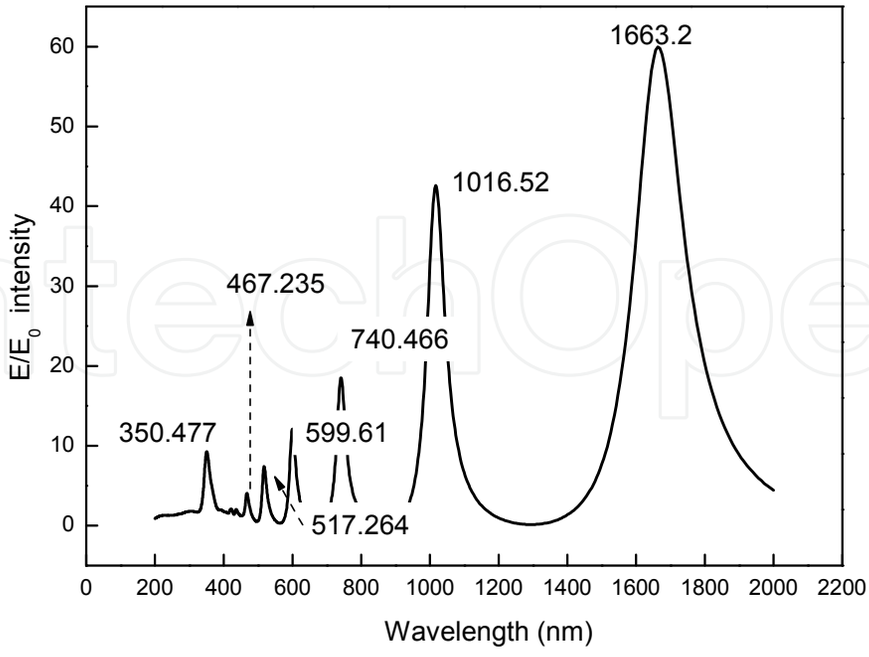

Figure 7. Multiple resonance spectrum around a silver nanowire. The resonance is shown as a value of |E|/|E$_0$| at a point of 5 nm above the nanowire as a function of wavelength of incident light (200 nm to 2000 nm).

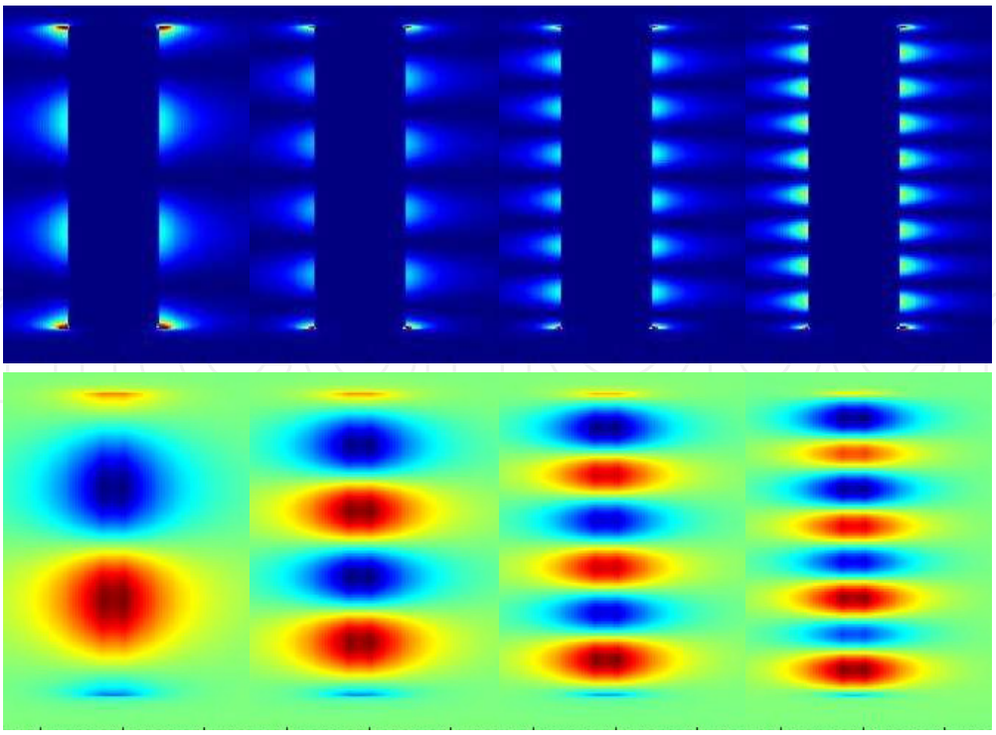

Figure 8. Simulated results for electric field profiles (top four panels) and vertical components of the Poynting vector of antenna radiations (bottom four panels) around a silver nanowire, corresponding to the antenna mode (3λ/2, 5λ/2, 7λ/2 and 9λ/2 resonances). The electric field profile running through the center of the nanowires and the Poynting vector calculated at 55 nm above the nanowire axis.

3.5. Ti nanowire

Figure 9 and 10 show the calculated result of amplitude enhancement, electric field profile and poynting vector as a function of wavelength for Ti nanowire. In the spectral range of calculation a feature of the Ti nanowires is the broaden peaks and weak field distribution as compared to perfectly conducting and Ag nanowire structures.

When comparing the field enhancement vs. wavelength for the silver and titanium nanowires to the perfect conducting nanowire, we can understand the optical antennas based on the background of both well-developed radiowave antenna engineering and the plasmonic behavior. According to the classical antenna theory that a fundamental mode occurs when an antenna length is half of the wavelength (λ/2), the fundamental antenna mode (λ/2 resonance) for a 2000 nm long perfect conducting nanowire is around 4000 nm, the observed modes (A-D) shown in Figures 5 and 6 should be assigned as higher harmonic modes (3λ/2, 5λ/2, 7λ/2, and 9λ/2 resonances). Comparing the multiple resonances spectrum between the perfect conducting and silver nanowires (Figures 7 and 8), it can be pointed out that a silver nanowire is a superb candidate for broadband optical antenna, which support four harmonic resonance modes in spectral range 517 to 1663 nm and one surface plasmon resonance (SPR) at 350.477 nm, as shown in Figure 11. The silver nanowire antenna is a one-dimensional SPR cavity, support the plasmon mode by reflecting the SPR currents at both ends of the nanowires.

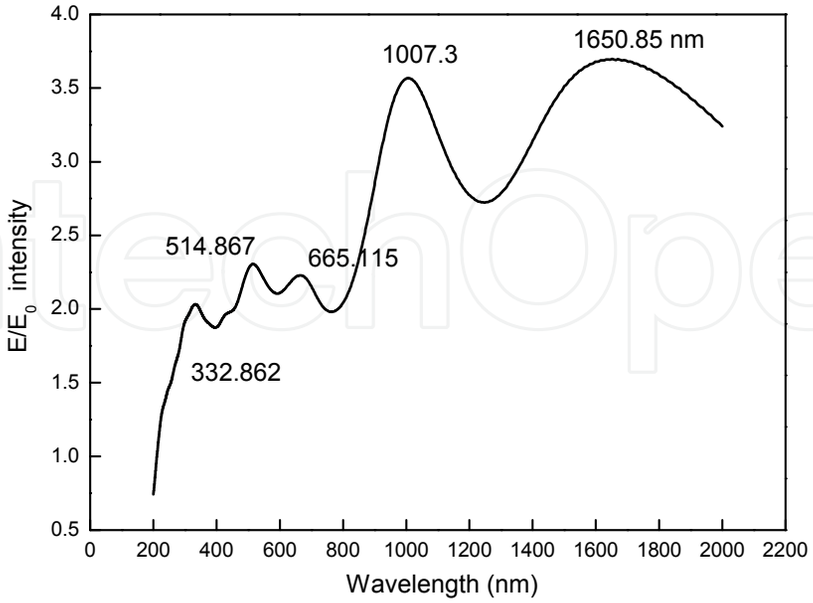

Figure 9. Multiple resonance spectrum around a titanium nanowire. The resonance is shown as a value of $|E|/|E_0|$ at a point of 5 nm above the nanowire as a function of wavelength of incident light (200 nm to 2000 nm).

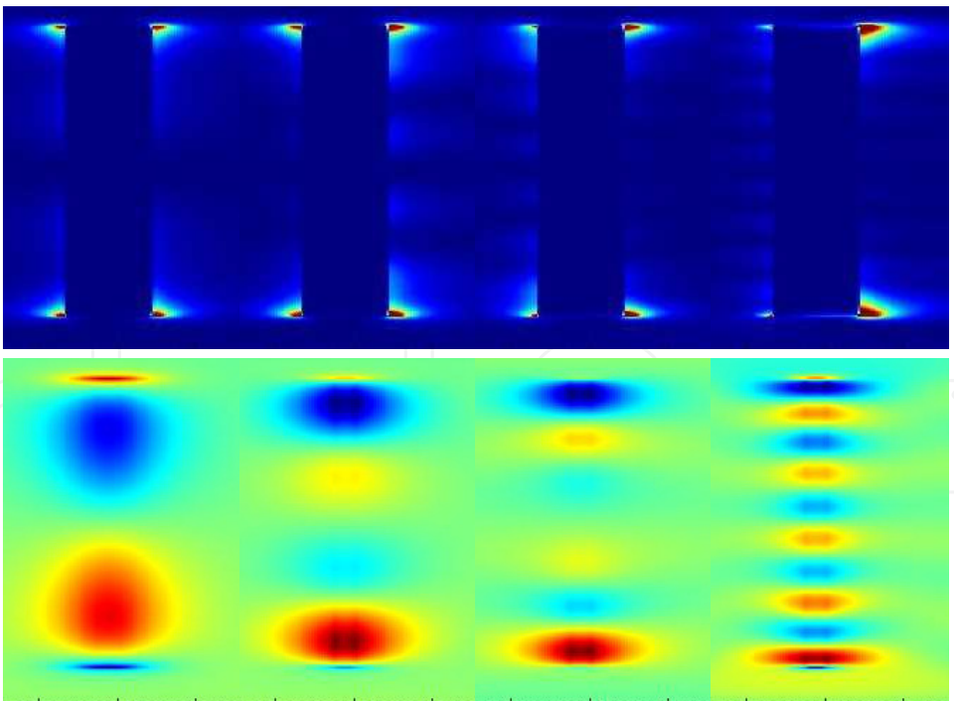

Figure 10. Simulated results for electric field profiles (top four panels) and vertical components of the Poynting vector of antenna radiations (bottom four panels) around a 2000 nm long titanium nanowire, corresponding to the antenna mode ($3\lambda/2$, $5\lambda/2$, $7\lambda/2$ and $9\lambda/2$ resonances). The electric field profile running through the center of the nanowires and the Poynting vector calculated at 55 nm above the nanowire axis.

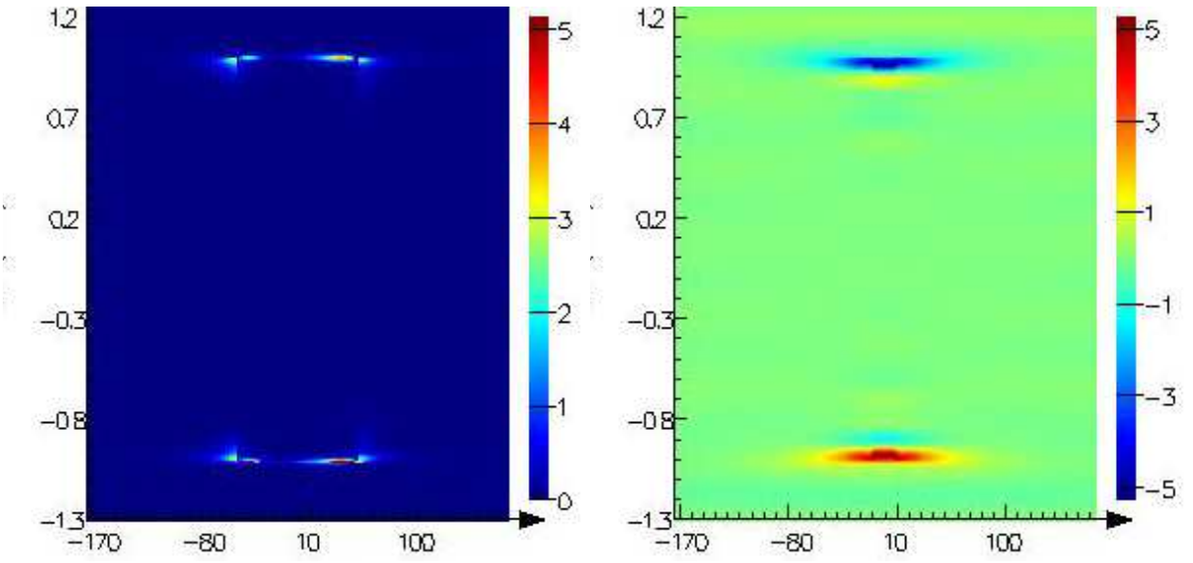

Figure 11. The electric field profiles (left) and vertical components of the Poynting vector of antenna radiations (right) around a silver nanowire at 350.477 nm.

For the titanium nanowire (Figures 9 and 10), their $|E|/|E_0|$ profiles and Poynting vector components are much weaker than the perfect conducting and silver nanowires, the possible research is that titanium has interband electronic transition at visible range [32]. The noble metals silver has higher energy of interband transitions 3.8ev (326nm) with respect to its surface plasmon resonance energy 3.38 eV (350nm) which reduces the damping and enhances the appearance of the plasmon mode, however, the transition metal titanium has lower energy of interband transition 2.0ev (610nm) which is liable for strong damping.

3.6. Ag-TiO_2-Ag MIM nanostructures

The end to end coupling of two nanowires with a small distance between them can create highly localized and strongly enhanced optical fields in the gap and due to this phenomenon such structures are well competent for optical antenna. The coupling between two nanowire antennas robustly increases with decreasing the gap distance. To study this effect in the spectral response and its intensity enhancement we therefore calculated the symmetric and asymmetric metal-insulator-metal (MIM) nanostructures

MIM nanostructures were theoretically investigated as model systems for split-dipole optical antennas. Figure 4(b) shows the geometry of the heteronanowire structure. The heteronanowire is a split-dipole nanoantennas consisting of a silver nanowire (diameter, 100 nm) and identical titanium (Ti) nanowire with the length of 950 nm, aligned on the long axis along the dimer symmetric axes. The gap in the dimer is bridged by the titania (TiO_2) nanowire with the same diameter and 100 nm in length. The position p1 are 5 nm from the heterodimer apex, and the point p2 is at the middle of the titania nanowire. The nanoantenna-insulator-metal substrate structure imitated the nanorectenna, where an ac voltage could generate in the insulator and stimulate a tunnel current in an asymmetric

MIM tunneling diode. To observe the antenna electric-field profiles, full-field finite-difference-time-domain (FDTD) electromagnetic simulations were carried out for Ag-TiO_2-Ag and an Ag-TiO_2-Ti asymmetric MIM nanostructure under plane wave excitation.

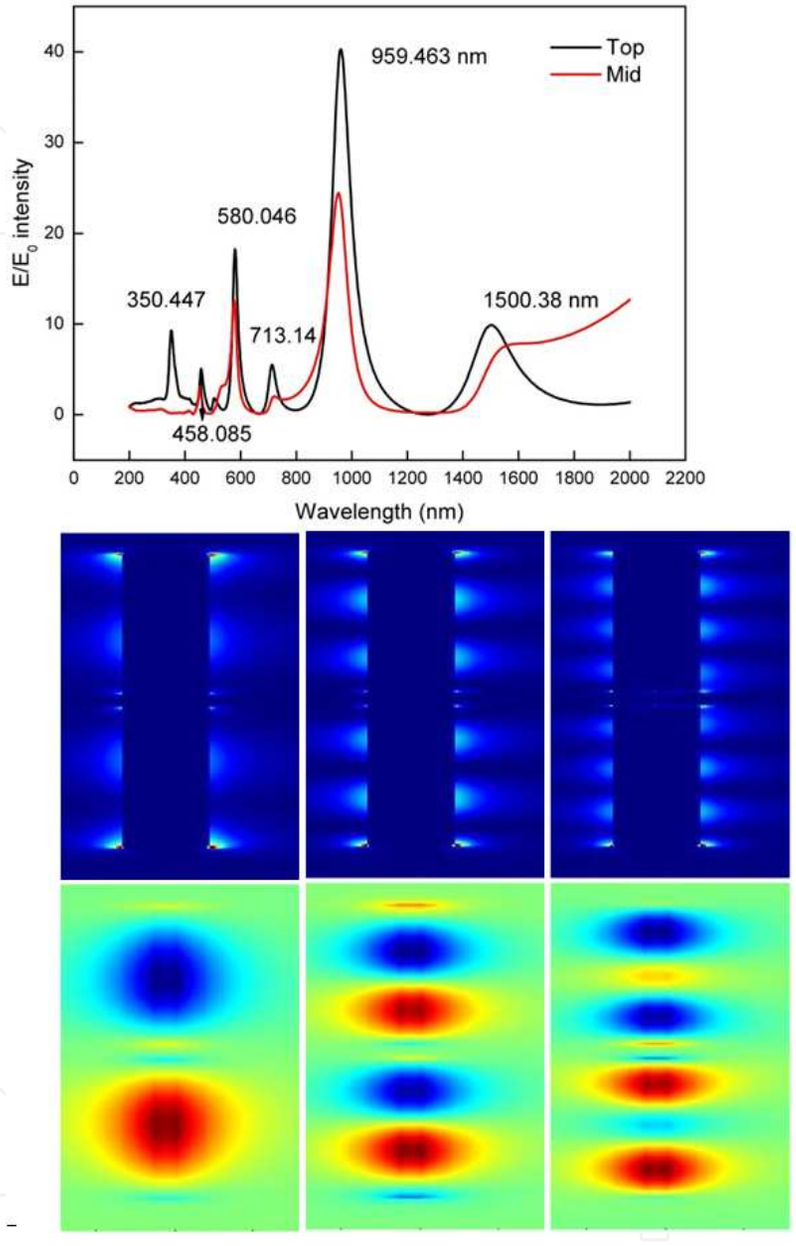

Figure 12. Resonance spectrum around a Ag-TiO_2-Ag MIM nanostructure shown as a value of $|E|/|E_0|$ at a point of 5 nm on top and in the middle of the homodimer as a function of wavelength (upper panel), the electric field profiles (middle panel) and vertical components of the Poynting vector of antenna radiations (bottom panel) corresponding to the antenna mode ($\lambda/2$, $3\lambda/2$, and $5\lambda/2$ resonances)

Figure 12 shows the local field enhancement spectra along with field profile and poynting vector component for the Ag-TiO_2-Ag symmetric. The Ag-TiO_2-Ag nanostructure is resonant at wavelength of 1500.38 nm, 959.463 nm and 713.14 nm and etc, corresponding to the first three order of the antenna resonances, and the near-field profiles at these $\lambda/2$, $3\lambda/2$ and $5\lambda/2$

resonances antenna mode are viewed from the electric field profiles and vertical components of the Poynting vector of antenna radiations. The near-field profiles clearly show that the electric field of the 2000 nm long Ag-TiO_2-Ag MIM antenna has a standing wave pattern, which is quite similar to that of single Ag nanowire antenna with 2000 nm length, their antenna radiations along the nanowires have same number of lobes and the lobe spacing of the fundamental mode is a little enlarged in the MIM antenna due to the gap between nanowires.

3.7. Ag-TiO_2-Ti MIM nanostructures

For asymmetric Ag-TiO_2-Ti MIM nanostructure, we also calculated the electric field, filed amplitude enhancement and vertical component of the Poynting vector antenna radiation corresponding to resonance modes, and the results are presented in Figure 13. It can be seen that the Ag-TiO_2-Ti nanostructure is resonant at wavelength of 1401.05 nm, 914.077 nm and 683.527 nm and etc, corresponding to the $\lambda/2$, $3\lambda/2$ and $5\lambda/2$ resonances antenna mode and the near-field profiles at first three order of the antenna resonances shows that the main contribution of the dimer antenna intensity field enhancement and field distribution are from silver in the asymmetric dimer.

For the Ag-TiO_2-Ti MIM antenna, the electric field is dominated by the Ag nanowires, the antenna radiations along the Ag nanowire of the MIM structure have same lobe patterns to the single Ag nanowire antenna with 950 nm lengths, and a fundamental antenna mode $\lambda/2$ can be identified unambiguously at the wavelength of 1401.25 nm. The electric field enhancement is bigger at the second harmonic mode ($3\lambda/2$) and reaches up to 22 and 7.5 in the middle of 100 nm thick TiO_2 insulators for the Ag-TiO_2-Ag and Ag-TiO_2-Ti MIM structures.

4. Optical rectification properties of metal-insulator-metal (MIM) devices

4.1. Review of metal-insulator-metal (MIM) diodes

The characterization and design of the optical rectification device focus mainly on the following areas:

1. The antenna;
2. The rectifier;
3. System integration.

The rectifier can transform an ac voltage to a dc voltage by means of a non-linear device, such as diode. To convert electromagnetic energy efficiently, a diode should be coplanar and couple to an optical antenna in order to take full advantage of the enhanced electric-field at the top of the metal electrodes or in the center gap of the antenna. Schottky diodes are routinely used in high frequency rectifiers because of their fast response time. These diodes have an operating frequency upper limit of approximately 3 THz, which is far below visible light frequencies. Antenna-couple metal-insulator-metal (MIM) diodes have been the subject of increasing interest due to their small size, CMOS compatibility, and ability to offer full

functionality without cooling and applied bias [33-36]. The diode of choice for the optical frequency rectifier is a metal-insulator-metal (MIM) diode, it is previously considered that these diodes are the fastest available diodes for detection in the optical region.

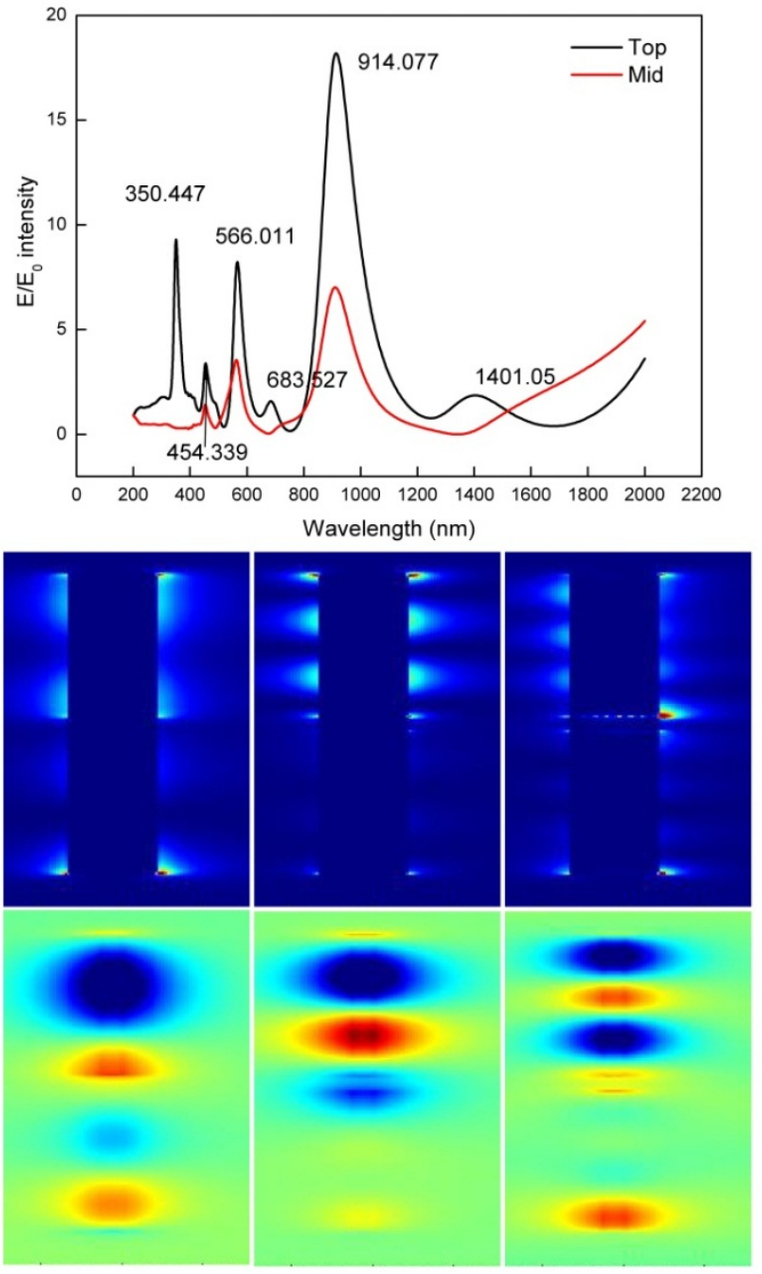

Figure 13. Resonance spectrum around a Ag-TiO_2-Ti MIM nanostructure shown as a value of $|E|/|E_0|$ at a point of 5 nm on top and in the middle of the heterodimer as a function of wavelength (upper panel), the electric field profiles (middle panel) and vertical components of the Poynting vector of antenna radiations (bottom panel) corresponding to the antenna mode ($\lambda/2$, $3\lambda/2$, and $5\lambda/2$ resonances)

However, plasmon absorption in metal-TiO_2 Schottky diode structures have recently been applied to photovoltaic devices [37, 38] and photocatalysts [39, 40] in the UV-visible and wavelength range, and an enhanced light harvesting property and a visible-light-induced

charge separation are obtained for the benefit of the metal nanoparticles. Furthermore, different explanations have been presented about the role of metal nanoparticles in the observed improvement in light conversion efficiency. These include (i) metal nanoparticles increased absorption due to surface plasmons and light trapping effects [41], (ii) metal nanoparticles functioned as electron donor promoting electron transfer from metal to semiconductor [37, 38, 42] and (iii) metal nanoparticles served as electron trapping media that can minimize the surface charge recombination in semiconductor [43 , 44].

Meanwhile, two main mechanisms have been mentioned for the electron transfer between the metal nanoparticle and the semiconductor during the energy conversion process. First, Tatsuma et al. [37, 38, 45] and other workers [42, 46] proposed that the photoexcited electrons in the metal nanoparticles transferred from the metal particle to the TiO_2 conduction band since the photoresponse of these metal-TiO_2 diode structures was consistent with the absorption spectra of Au or Ag nanoparticles. Second, Kamat et al [43, 44] and Li et al. [47] have suggested that the noble metal nanoparticles act as electron sinks or traps in the metal-TiO_2 diode structures to accumulate the photogenerated electrons, which could minimize charge recombination in the semiconductor films. Obviously, a better understanding of these effects is crucial in exploiting the beneficial aspects of metal nanoparticles in photovoltaics.

In this section, we modeled and fabricated a MIM diode located at the mid-point of an Ag-TiO_2-Ti MIM antenna. The photodeposition was used to synthesis Ag-Cu nanoparticles in the TiO_2 nanotube grown from Ti foils to obtain the AgCu-TiO_2/Ti MIM diode structures, and their photoelectronic properties were measured under simulated sunlight and visible light. The Schottky barrier analyses indicated that the electron transport direction was the electrons transferred from metal nanoparticles to TiO_2.

4.2. Theoretical modeling of Ag-TiO_2-Ti MIM diodes

As shown in Figure 14, a MIM diode consists of three sections: a polished metal on a substrate as the base (anode), a natural oxide layer as the insulator (barrier), and another metal layer (cathode). When the barrier layer is extremely thin (10 to 50 Å), some quantum confinement effects may result in the tunnelling of electrons through the insulator layer. In this device, metals are treated as perfect electrical conductors, and are assumed to be in thermal equilibrium. Typically, the electrons in the metal are driven out of equilibrium by the absorbed power. The absorbed photons energize the electrons in the metal, allowing them to overcome the Schottky barrier and be collected in the cathode, eventually leaving through the back contact as measured current.

However, in these recent metal-TiO_2 Schottky diode structures [37-47], it would appear that the barrier layer was actually quite a bit thicker than 10 nm (probably in excess of 1 um) and further details was unable to be found in these papers. Semi-classical models did not account for non-equilibrium energy distributions of carriers, or do so through a localize lattice temperature. This problem in general is difficult for a traditional drift-diffusion

model to capture the plasmonic effect in the illuminated metal layer. The logical approach to modeling the MIM rectifier would be to start with a customary potential-energy diagram.

Figure 14 shows the energy-band diagram of an Ag-TiO_2-Ti MIM diode. For smooth electron transportation through the interface between the semiconductor TiO_2 and the metal electrodes, an intervening ohmic contact is necessary. Since TiO_2 is an n-type semiconductor and its conduction band level is close to 4.2 eV, the electron affinity of TiO_2 is little greater than 4.2 eV, the work function of Ti is 4.33 eV, and the Ti-TiO_2 interface therefore becomes Schottky contact. Ohmic contact can be formed using Ag with the work function of 4.0 eV.

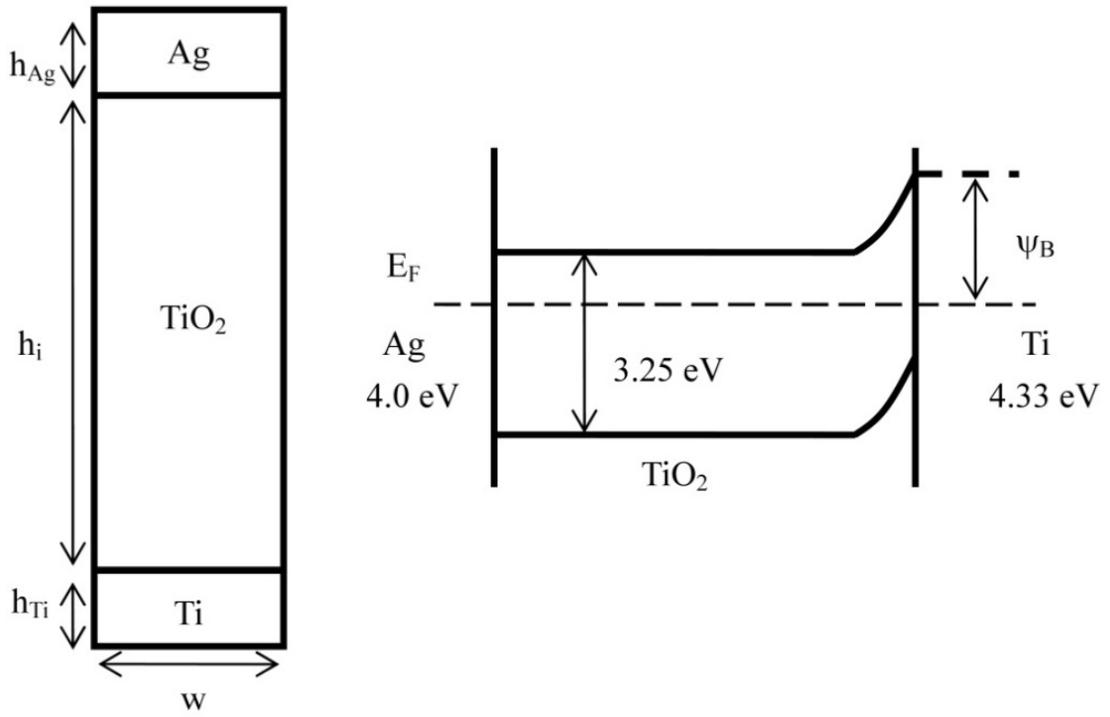

Figure 14. Energy-band diagram of a Ag-TiO_2-Ti MIM diode. Two MIM diodes are considered here, one is conventional diode with the diameter w= 2 μm, the TiO_2 layer thickness h_i = 60 μm, and the metal electrode thickness $h_{Ag} = h_{Ti}$ = 2 μm, the other is MIM nanodiode with the diameter w= 100 nm, the TiO_2 layer thickness h_i = 100 nm, and metal electrode thickness $h_{Ag} = h_{Ti}$ = 100 nm.

In order to understand the electron transport properties in the Ag-TiO_2-Ti MIM nanodiode, we performed the two-dimensional finite element (FEM) calculation based on the drift and diffusion equation for electrons and holes. In Figure 15, the calculated I-V curves are depicted for a conventional diode (a) and a MIM nanodiode (b) under various n-doping concentrations. It is show that the I-V curves show clear nonlinear and asymmetric current characteristic. The nonlinearity of current is basic mechanism for the rectification of an incident wave to a DC output.

As shown in Figure 15(a), for a conventional Ag-TiO_2-Ti MIM diode, the high doping leads to the high current density at zero bias. When doping is added, it will shift the Fermi level in the TiO_2, which will then define the Schottky barrier height (SBH) at the Ti-TiO_2 interface, the greater SBH results in larger charge transfer across metal-semiconductors interface,

creating a large potential drop across depletion width and allowing a more efficient collection of electrons and holes.

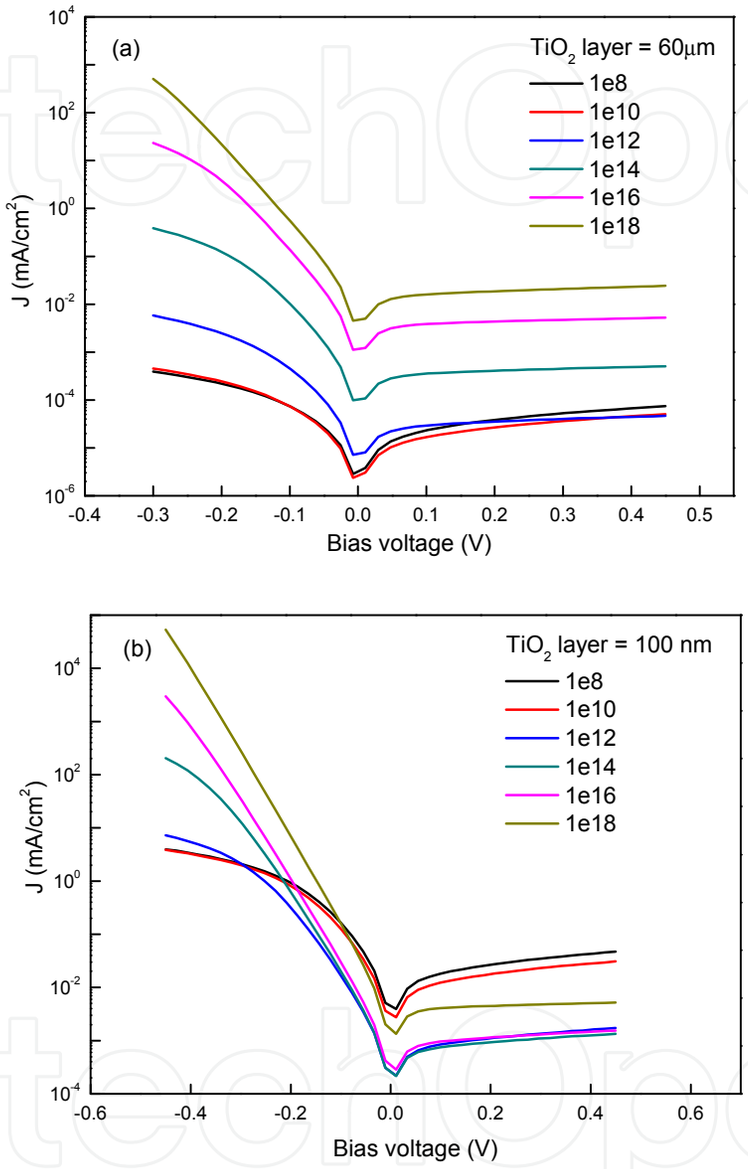

Figure 15. Simulated I-V characteristic for the Ag-TiO_2-Ti MIM diode. (a) is conventional diode with the diameter w= 2 μm, the TiO_2 layer thickness h_i = 60 μm, and the metal electrode thickness $h_{Ag} = h_{Ti}$ = 2 μm; (b) is MIM nanodiode with the diameter w= 100 nm, the TiO_2 layer thickness h_i = 100 nm, and the metal electrode thickness $h_{Ag} = h_{Ti}$ = 100 nm.

4.3. Experimental work of AgCu-TiO_2/Ti MIM nanostructures

The AgCu-TiO_2/Ti MIM nanoantenna heterostructures were fabricated using an electrochemical process and several measurements were carried out to determine if the MIM

diode was producing direct current through plasmonic rectenna action. The TiO_2 nanotube layer was grown by anodizing 300-600 nm of titanium [48] on which the bimetallic Ag-Cu nanoparticle film were deposited using a photodeposition method. We chose the bimetallic Ag-Cu nanoparticles as the plasmonic medium where Cu alloying was used to prevent the natural oxidation of the silver nanoparticles and keep its good plasmonic property [49-51]. The surface morphologies of samples were characterized by scanning electron microscopy (JSM, 6390A) with energy dispersive X-ray spectroscopy (SEM-EDS). The photocurrent density - voltage curves (J-V) were measured at a potential sweep rate of 10 mV/s, with the Pt net as counter electrode, and a saturated calomel electrode (SCE) as reference electrode. Electrochemical Impedance Spectroscopy (EIS) was used to evaluate the properties of the different electrodes under AC polarization. The frequency range was 0.1 Hz to 100 kHz for amplitude of 5 mV in a DC potential of –0.2 V_{SCE}.

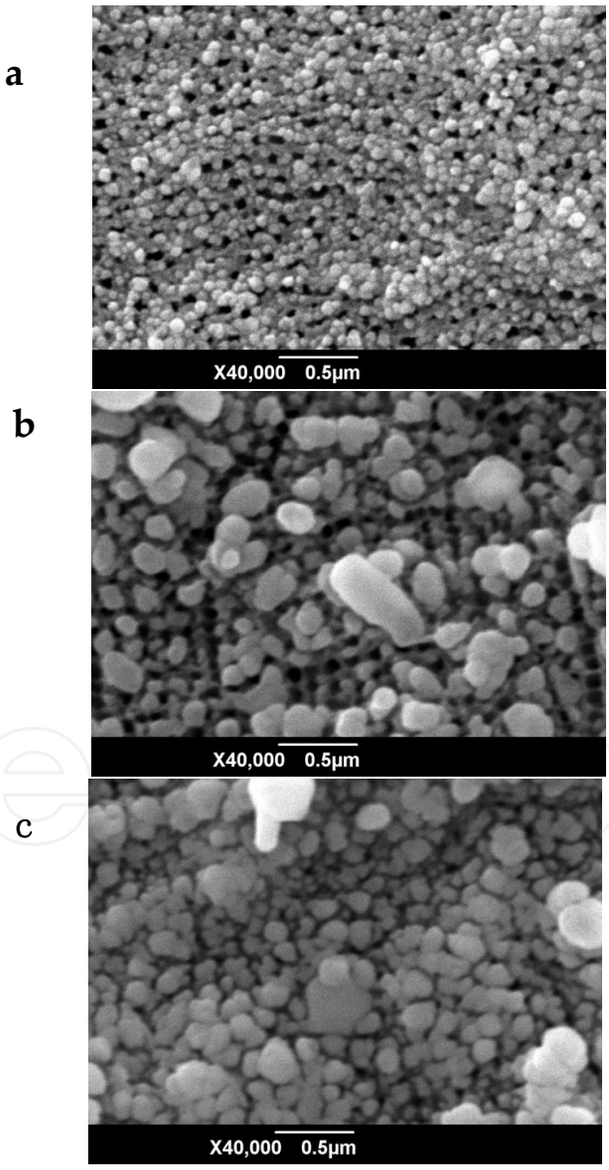

Figure 16. SEM images of Cu (a), Ag (b) and Ag-Cu (c) nanoparticle layer deposited on TiO_2/Ti substrate.

Figure 16 (a, b and c) shows the surface morphology of the Cu, Ag and Ag-Cu nanoparticles deposited on TiO_2 nanotube, respectively. The Cu nanoparticles were evenly and densely distributed on the surface of TiO_2 nanotube layer, the measured nanoparticle size ranged 46 nm to 120 nm. The Ag nanoparticles are bigger than Cu nanoparticles and are not in uniform size with the big ones over 500 nm and the small ones below 100 nm. The possible reason is that the standard electrode potential of Ag^+/Ag^0 (0.78 eV) is higher than that of Cu^{2+}/Cu^0 (0.34 eV), so Ag^+ is reduced more rapidly and grows faster than Cu^{2+}. For the surface morphology of the Ag-Cu nanoparticles on TiO_2 nanotube layers, it is obvious that the Ag-Cu nanoparticles were denser than Ag nanoparticles. The energy dispersive X-ray spectroscopy (EDS) show that the atom ratios of Ag to Cu was 1.68:3.72 and the Cu content was less than that in the electrolyte because the reduced Cu can be further oxidized by Ag^+. Actually, this galvanic reaction has a dominated effect on the formation of Ag-Cu nanoparticles. Once the Cu nanoparticles formed firstly, the Ag^+ will be reduced at the surface of Cu nanoparticles and form the core-shell structure, an alloyed Ag-Cu nanoparticles formed after the reductive reaction and the atomic mutual diffusion at the interface of Cu and Ag atoms.

Figure 17 shows the measured J-V curves under simulated sunlight and visible light for the AgCu-TiO_2/Ti MIM structure, which had a short current density of -1.201 mA/cm^2 under simulated sunlight, and decreased to -0.734 mA/cm^2 under visible light, indicating that Ag-Cu nanoparticles were very photosensitive to the UV light.

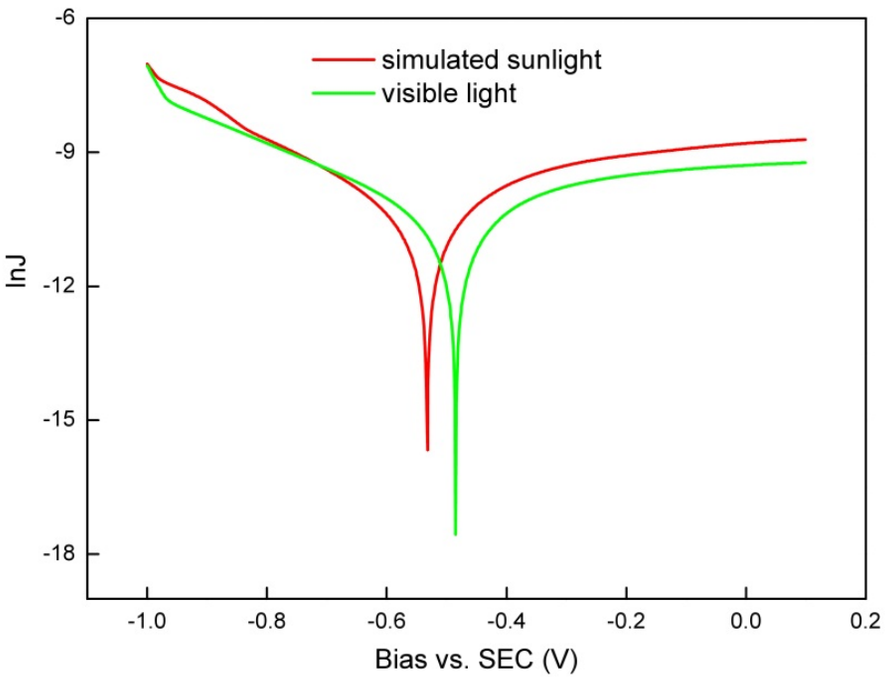

Figure 17. Measured current density and voltage (J-V) curves for the AgCu-TiO_2/Ti MIM structure under visible light and under simulated sunlight. The applied bias is versus the saturated calomel electrode (SCE).

The work function difference between the metal and the n-TiO_2 results in electrons transferred from TiO_2 to the metal nanoparticles yielding a Schottky junction. We can determine the electron transport direction by comparing the SBH changes under different irradiation conditions. The SBH values were calculated in lnJ-V diagram shown in Figure 17 by the following Equation:

$$J_s = A^* T^2 \exp(-q\phi_{SBH} / k_B T) \quad (1)$$

where ϕ_{SBH} is SBH at the zero bias, A^* is the Richardson constant, k_B is the Boltzmann constant, and J_s is the zero bias saturation current density. The calculated SBH values were 1.021eV and 1.006 eV for the simulated sunlight and under visible light irradiations, *i.e.*, the ϕ_{SBH} values calculated under the simulated sunlight are higher than that measured under visible light and less electrons were produced and transferred to TiO_2 under visible light. This result clearly indicates that the metal nanoparticles can be photoexcited as electron donors, and that the electrons transferred from metal nanoparticles to TiO_2.

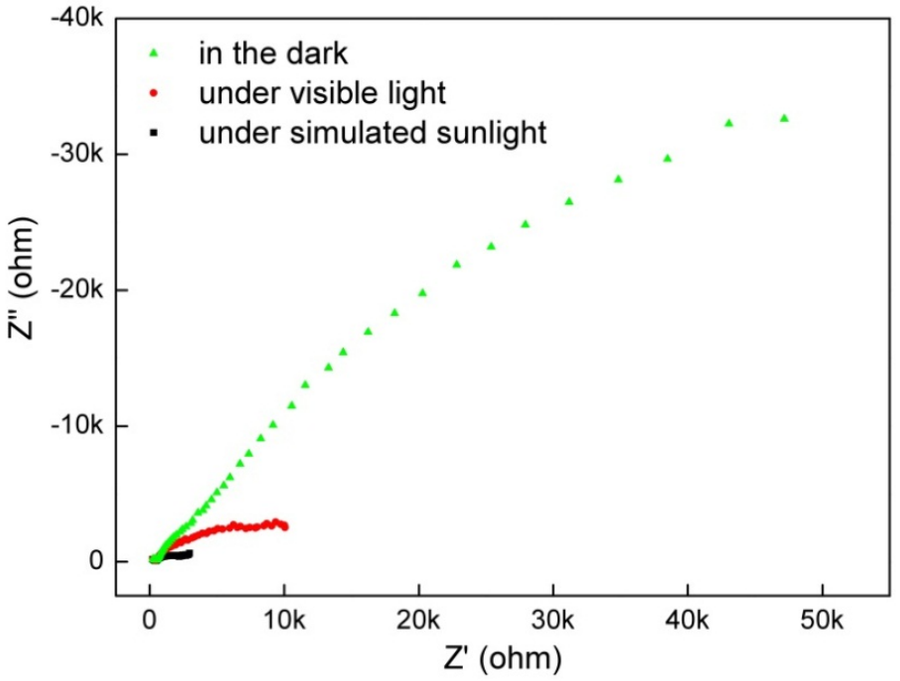

Figure 18. Nyquist diagram measured for the AgCu-TiO_2/Ti MIM structure under simulated sunlight, visible light, and in the dark.

Figure 18 exhibits that impedance measured under simulated sunlight and visible light were sharply decreased in comparison with that measured in the dark at the low frequency region (< 100Hz), indicating a decrease of charge transfer resistance. This can be justified by the bending of the impedance arc in the low frequency region (the second arc) in the Nyquist diagram, because the bending of the arc in this region indicated a process of charge transfer while the linear relationship between the imaginary and real component of the impedance mean a diffusion process controlled step. Among the three photoelectrodes, the low frequency region arc of the AgCu-TiO_2/Ti MIM structure was largely bended under

both light irradiations, which indicated that faster charge transfer was obtained in the AgCu-TiO_2/Ti diode.

5. Summary

The plasmonic effect of the metal nanostructure has been explored to improve the conversion efficiency for DSSCs. We found that metal nanoparticles in the plasmonic DSSC can lead to serious parasitic absorption even under the optimized conditions, the absorption of metal nanoparticles takes up about 20–30% of the total absorption of the DSSC at visible wavelengths. To solve the problem of the metal parasitic absorption in the DSSC caused by the surface plasmon optical effect, designing and fabricating metal-insulator-metal sandwich structure as photon acceptor and electron donor may be a research direction for the further development of the plasmonic photovoltaic techniques.

The metal-insulator-metal (MIM) nanostructures were theoretically investigated as model systems for optical antennas. The field enhancements vs. wavelength for the silver and titanium nanowires with 2000 nm length have shown the higher harmonic modes ($3\lambda/2$, $5\lambda/2$, $7\lambda/2$, and $9\lambda/2$ resonances). A silver nanowire is a superb candidate for broadband optical antenna, which support four harmonic resonance modes in spectral range 517 to 1663 nm and one surface plasmon resonance (SPR) at 350.477 nm. The Ag nanowires dominated the electric field for the Ag-TiO_2-Ti MIM antenna.

The current density and voltage curves of Ag-TiO_2-Ti (MIM) nanostructure have been modeled at the micrometer and nanometer scale. We are carrying out experiments on the optical rectification properties of AgCu-TiO_2/Ti metal-insulator-metal (MIM) diode devices. Cu, Ag, and Ag-Cu nanoparticle films exhibits different morphological characters. The measured J-V curves under simulated sunlight and visible light for the AgCu-TiO_2/Ti MIM structure exhibit a short current density of -1.201 mA/cm^2 under simulated sunlight, and decreased to -0.734 mA/cm^2 under visible light, indicating that the electrons transferred from metal nanoparticles to TiO_2 layer.

Author details

Fuyi Chen*, Jian Liu and Negash Alemu
State Key Laboratory of Solidification Processing,
Northwestern Polytechnical University, Xian, China

Acknowledgement

This study was supported by the National Natural Science Foundation of China (Grant Nos. 50971100 and 50671082), the Research Fund of State Key Laboratory of Solidification Processing in China (Grant No. 30-TP-2009), and the NPU Foundation for Fundamental Research (Grant No. NPU-FFR-ZC200931).

* Corresponding Author

6. References

[1] Takamoto T, Kaneiwa M, Imaizumi M, et al. InGaP/GaAs-based Multijunction Solar Cells. Progress in Photovoltaics 2005; 13(6) 495-511

[2] Nazeeruddin M K, DeAngelis F, Fantacci S, Selloni A, Viscardi G, Liska P, Ito S, Takeru B, Gratzel B M. Combined Experimental and DFT-TDDFT Computational Study of Photoelectrochemical Cell Ruthenium Sensitizers. Journal of American Chemistry Society 2005; 127(48)16835-16847

[3] O'Regan B, Gratzel M, A Low-cost, High-efficiency Solar Cell Based on Dye-sensitized Colloidal TiO_2 Films. Nature 1991; 353(24)737-739

[4] Stuart H R, Hall D G. Island Size Effects in Nanoparticle-enhanced Photodetectors. Applied Physics Letters 1998; 73, 3815,

[5] Atwater H A, Polman A. Plasmonics for Improved Photovoltaic Device. Nature Materials 2010; 9,205-213

[6] Ferry V E, Munday J N, Atwater H A. Design Consideration for Plasmonic Photovoltaics. Advanced Materials 2010; 22, 4794-4808

[7] Brown M D, Suteewong T, Kumar R S S, Innocenzo V D, Petrozza A, Lee M M, Wiesner U, Snaith H J. Plasmonic Dye-sensitized Solar Cells Using Core-shell Metal-insulator Nanoparticles. Nano Letters 2011; 11(2)438-445

[8] Hagglund C, Zach M, and Kasemo B. Enhanced Charge Carrier Generation in Dye sensitized Solar Cells by Nanoparticle Plasmons. Applied Physics Letters 2008; 92, 013113

[9] Du S, Li Z. Enhanced Light Absorption of TiO_2 in the Near-ultraviolet Band by Au Nanoparticles. Optics Letters 2010; 35(20)3402-3404

[10] Guilatt O, Apter B, Efron U, Light Absorption Enhancement in Thin Silicon Film by Embedded Metallic Nanoshells. Optics Letters 2010; 35(8)1139-1141

[11] Fu D, Zhang X, Barber R L and Bach U. Dye-sensitized Back-contact Solar Cells. Advanced Materials 2010; 22, 4270–4274

[12] Durr M, Menges B, Knoll W, Yasuda A, and Nelles G. Direct Measurement of Increased Light Intensity in Optical Waveguides Coupled to a Surface Plasmon Spectroscopy setup. Applied Physics Letters 2007; 91, 021113

[13] Atwater H A, Polman A. Plasmonics for Improved Photovoltaic Device. Nature Materials 2010; 9,205-213

[14] Yuan L, Chen F Y, Zheng C F, Liu J, Alemu N. Parasitic Absorption Effect of Metal Nanoparticles in the Dye-sensitized Solar Cells. Physica Status Solidi A 2012; 209,1376-1379.

[15] Robinson J and Rahmat-Samii Y. Particle Swarm Optimization in Electromagnetics. IEEE Transaction on Antennas and Propagation 2004; 52, 397.

[16] Robinson J, Sinton S and Rahmat-Samii Y. Particle Swarm, Genetic Algorithm, and their Hybrids: Optimization of a Profiled Corrugated Horn Antenna. In: Proc. IEEE Int. Symp. Antennas Propagation, San Antonio, TX, 1(314-317), 2002

[17] O'Regan B, Gratzel M. A Low-cost, High-efficiency Solar Cell Based on Dye-sensitized Colloidal TiO_2 Films. Nature 1991; 353,737

[18] Green M A and Pillai S. Harnessing Plasmonics for Solar Cells. Nature Photonics 2012; 6, 130

[19] Schuck P J, Fromm D P, Sundaramurthy A, Kino G S, Moerner W E. Improving the Mismatch between Light and Nanoscale Objects with Gold Bowtie Nanoantennas. Physics Review Letters 2005; 94, 017402

[20] Muhlschlege P, Eisler H, Martin O, Hecht B, Pohl D. Resonant Optical Antennas. Science 2005; 308, 1607-1609

[21] Novotny L, van Hulst N. Antennas for Light. Nature Photonics 2011; 5, 83-90,

[22] Brown W C. The history of Power Transmission by Radio Waves. IEEE Transactions on Microwave Theory and Techniques 1984; 32(9)1230-1242

[23] Brown W C. Optimization of the Efficiency and other Properties of the rectenna element. IN: 1976 IEEE-MTT-S International Microwave Symposium, 142-144, 1976

[24] Hocker L O, Sokoloff D R, Daneu V, Szoke A and Javan A. Frequency Mixing in the Infrared and Far-infrared using a Metal-to-metal Point Contact Diode. Applied Physics Letters 1968; 12, 401-402

[25] Matarrese L M and Evenson K M. Improved Coupling to Infrared Whisker Diodes by Use of Antenna Theory. Applied Physics Letters 1970; 17, 8-10

[26] Fetterman H R, Clifton B J, Tannenwald P E and Parker C D. Submillimeter detection and mixing using Schottky diodes. Applied Physics Letters 1974; 24, 70

[27] Fetterman H R, Tannenwald P E, Clifton B J, Parker C D, Fitzgerald W D and Erickson N R. Far-ir Heterodyne Radiometric Measurements with Quasioptical Schottky Diode Mixers. Applied Physics Letters 1978; 33, 151

[28] Small J G, Elchinger G M, Javan A, Sanchez A, Bachner F J and Smythe D L, An Electron Tunnelling at Infrared Frequencies: Thin-film M-O-M Diode Structure with Broad-band Characteristics. Applied Physics Letters 1974; 24,275-279

[29] Gustafson T K, Schmidt R V, and Perucca J R. Optical Detection in Thin-film metal - oxide - metal diodes. Applied Physics Letters 1974; 24, 620

[30] Bailey R L. A Proposed New for a Solar-energy Converter. Journal of Engineering for Power 1972; 94, 73-77

[31] Marks A M. Device for Light Power to Electric Power. U.S. Patent 4 445 050, 1984

[32] Chen F Y, Alemu N, Johnston R L. Collective Plasmon Modes in a Compositionally Asymmetric Nanoparticle Dimer. AIP Advances 2011; 1,302134

[33] Fumeaux C, Herrmann W, Rothuizen H, De Natale P and Kneubühl F K. Mixing of 30 THz Laser Radiation with Nanometer Thin Film Ni-NiO-Ni Diodes and Integrated Bow-tie antennas. Applied Physics B Laser and Optics 1996; 63(2)135–140.

[34] Codreanu I, González F and Boreman G. Detection Mechanisms in Microstrip Dipole Antenna-coupled Infrared Detectors. Infrared Physics and Technology 2003; 44(3)155–163.

[35] Hobbs P C, Laibowitz R B and Libsch F R. Ni-NiO-Ni Tunnel Junctions for Terahertz and Infrared Detection. Applied Optics 2005; 44(32)6813–6822

[36] Chen F Y, Yuan L, Johnston R. L. Low-loss Optical Magnetic Metamaterials on Ag-Au Bimetallic Fishnets. Journal of Magnetism and Magnetic Materials 2012; 324, 2625-2630.

[37] Tian Y, Tatsuma. T. Plasmon-induced Photoelectrochemistry at Metal Nanoparticles Supported on Nanoporous TiO_2. Chemistry Communication 2004; 16, 1810-1811.

[38] Tian Y, Tatsuma T. Mechanisms and Applications of Plasmon-Induced Charge Separation at TiO_2 Films Loaded with Gold Nanoparticles. Journal of American Chemistry Society 2005; 127, 7632-7637.

[39] Awazu K, Fujimaki M, Rockstuhl C, Tominaga J, Murakami H, Ohki Y, Yoshida N, Watanabe T A. Plasmonic Photocatalyst Consisting of Silver Nanoparticles Embedded in Titanium Dioxide. Journal of American Chemistry Society 2008; 130, 1676-1680

[40] Irie H, Kamiya K, Shibanuma T, Miura S, Tryk D A, Yokoyama T, Hashimoto K. Visible Light-Sensitive Cu(II)-Grafted TiO_2 Photocatalysts: Activities and X-ray Absorption Fine Structure Analyses. Journal of Physical and Chemistry C 2009; 113,10761–10766.

[41] Stuart H R and Hall D G. Island Size Effects in Nanoparticle-enhanced Photo Detectors. Applied Physics Letters 1998; 73, 3815-3817.

[42] Mubeen S, Hernandez-Sosa G, Moses D, Lee J, Moskovits M. Plasmonic Photosensitization of a Wide Band Gap Semiconductor: Converting Plasmons to Charge Carriers. Nano Letters 2011; 11, 5548–5552.

[43] Chandrasekharan N, Kamat P V. Improving the Photoelectrochemical Performance of Nanostructured TiO_2 Films by Adsorption of Gold Nanoparticles. Journal of Physical and Chemistry B 2000; 104, 10851–10857.

[44] Takai A, Kamat P V. Capture, Store, and Discharge. Shuttling Photogenerated Electrons across TiO_2 Silver Interface. ACS Nano 2011; 5, 7369-7376.

[45] Sakai N, Fujiwara Y, Takahashi Y, Tatsuma T. Plasmon-Resonance-Based Generation of Cathodic Photocurrent at Electrodeposited Gold Nanoparticles Coated with TiO_2 Films. ChemPhysChem 2009; 10, 766 – 769.

[46] Furube A, Du L, Hara K, Katoh R, Tachiya M. Ultrafast Plasmon-Induced Electron Transfer from Gold Nanodots into TiO_2 Nanoparticles. Journal of American Chemistry Society 2007; 129, 14852-14853.

[47] Liu L, Wang G, Li Y, Li Y, Zhang J. Z. CdSe Quantum Dot-Sensitized Au/TiO2 Hybrid Mesoporous Films and Their Enhanced Photoelectrochemical Performance. Nano Research 2011; 4, 249–258.

[48] Chen F Y, Liu J. A Plasmonic Rectenna and its Fabrication Method. Chinese Patent, 201210002179.5, 2012.

[49] Chen F Y, Zheng C F, A Silver-copper Nanoalloy and its Electrical Synthesis Method. Chinese Patent, 201110310987.3, 2011

[50] Chen F Y, Johnston R L. Charge Transfer Driven Surface Segregation of 13-atom Au-Ag Nanoalloy and its Relevance to Structural, Optical and Electronic properties. Acta Materialia 2008; 56, 2374-2380

[51] Chen F Y, Johnston R L. Energetic, Electronic and Thermal effects on Structural Properties of Ag-Au Nanoalloys. ACS Nano 2008; 2, 165-175

IntechOpen